RESEARCH

Frequency-Dependent Force Direction Elucidates Neural Control of Balance

Kaymie Shiozawa[1], Jongwoo Lee[1*], Marta Russo[3], Dagmar Sternad[3,4,5] and Neville Hogan[1,2]

Abstract

Background: Maintaining upright posture is an unstable task that requires control of translational and rotational motions. Humans use foot-ground interaction force, characterized by point of application, magnitude, and direction to manage body accelerations. Previous work identified a point of intersection of the foot-ground interaction force vectors that exhibited consistent frequency-dependent behavior.

Methods: To test whether this frequency-dependent behavior provided a distinctive signature of neural control or was a necessary consequence of biomechanics, this study simulated quiet standing and compared the results with human subject data. If a standing human was modeled as a single inverted pendulum, no controller could reproduce the experimentally observed frequency-dependence of the intersection point height. The simplest competent model that approximated a standing human was a double inverted pendulum with torque-actuated ankle and hip joints. It was stabilized by a linear feedback controller based on position and velocity errors of each joint.

Results: When the relative cost between state deviation and control effort was varied, the frequency at which the intersection point crossed the center of mass position shifted. A similar effect was obtained by varying the relative cost between the ankle and hip control effort. The relative strength of ankle and hip actuation noise added to the simulated system affected the intersection point height at high frequencies.

Conclusions: As a range of controller parameter sets could stabilize this model and produce the observed change in the vertical position of the intersection point with increasing frequency, the decrease in intersection point height appears to reflect a biomechanical constraint and not a consequence of control. Among the several controller parameter sets considered, that which best reproduced the human experimental results used minimal control effort and more ankle torque than hip torque. This suggests that the neural strategy employed by human subjects to maintain quiet standing balance engages at least two degrees of freedom and is best described by minimal control effort and emphasizing ankle torque.

Keywords: posture and balance; inverted pendulum model; ground reaction forces; neural control

*Correspondence: jw127@mit.edu

[1]Department of Mechanical Engineering, Massachusetts Institute of Technology, Cambridge, MA 02139, USA

Full list of author information is available at the end of the article

Background

Controlling balance during standing and walking is a fundamental necessity for human mobility. Although maintaining upright posture requires less movement than locomotion, its inherently unstable nature makes it an interesting neural sensorimotor control problem [1–3]. For this reason, the way humans maintain balance has been studied along several different avenues. For instance, conventional studies of human balance have focused on analyzing the trajectories of the center of mass and the center of pressure during quiet standing [4, 5]. However, studying the motion of the center of mass and the center of pressure without considering whole-body angular acceleration is insufficient to fully describe the complex dynamics and control of the multi-segmented human body. The ground reaction force and where it acts with respect to the center of mass give insight into how human subjects manipulate the net angular and translational motion of the body to maintain upright standing posture.

In particular, Gruben and colleagues studied the relation between ground reaction force and the center of pressure in human subjects during quiet standing and quantified a unique point of intersection of ground reaction force vectors [6, 7]. This intersection point was originally identified in the context of walking [8,9] and was first applied to standing balance by Gruben and colleagues. Because the height of the intersection point relative to the center of mass dictates the respective directions of translational and angular accelerations, it provides a compact geometric representation useful to understand the dynamics and control of human balance. When examining the force vectors in limited frequency bands, they found that the vertical position of the intersection point exhibited a consistent pattern across subjects: above the center of mass at low frequencies, decreasing as frequency increased, and reaching an asymptote below the center of mass at higher frequencies. With this observation, they suggested the existence of a neural controller which dictates the balance strategy and may consider factors such as efficiency and stability. However, gravito-inertial biomechanics plays an important role and might account for some of the variation of intersection point height with frequency. To clarify the possible roles of neural control and biomechanics, the study presented here modeled the details of the dependence of the intersection point on frequency as reported in human postural control [6].

Separating the neural contribution from biomechanical factors by only observing human motion is challenging. Here we used mathematical models to advance our understanding of the nature of neural control in balance and the extent to which it is constrained by biomechanics [2,3]. We further took advantage of optimal control theory, which enables a systematic search of the complicated space of possible controllers in a physiologically-plausible way that results in particular kinematic and kinetic patterns [3, 10, 11]. These patterns generate testable hypotheses about neural control schemes based on specific features of the postural control system [12, 13].

To assess the strategies of neural control and discriminate them from the dictates of biomechanics, this study simulated ground reaction forces during quiet standing by approximating a human body as an inverted pendulum. Although a single-degree-of-freedom inverted pendulum has been used in prior studies to model human quiet standing [14, 15], initial analysis clearly established that this model could not reproduce the observed decline of the intersection point height with frequency; a detailed analysis is presented in Appendix 1. With the goal of using the simplest model competent to account for experimental observations, we approximated a human body as a double inverted pendulum, i.e. one with two sagittal-plane degrees of freedom. This model is fully described by hip and an-

kle joint angles and velocities and is driven by corresponding joint torques. The internal perturbations that cause persistent sway in quiet standing were simulated by additive actuation noise.

Linear analysis can be justified as standing balance is a task that primarily exhibits small deviations about the upright position. Even with this simplification, the range of selectable controller parameters is daunting. Though only position and velocity feedback about each degree of freedom were considered, the space of system parameters to be selected has nine dimensions (eight controller gains and one ratio of noise strengths). To manage this complexity, a well-established approach to controller synthesis, the so-called Linear Quadratic Regulator (LQR) design [16], was applied to this work. This method determines an optimal compromise between deviations of system state variables (i.e. joint positions and velocities) from nominal values and deviations of control effort (i.e. joint torques) from zero. A particular advantage of this design procedure is that it *guarantees* a stable controller, even when control effort is confined to its minimum. This feature is especially advantageous to test a working hypothesis that neural strategies used in human balance economize effort. Previous use of linear quadratic optimal control has been insightful, for example, to understand the generation of a continuum of balance strategies in human standing in response to perturbation [12, 13].

With this approach, different effects of the stabilizing control parameters on the pattern of frequency-dependent variation of the intersection point were examined. Results indicated that, for all the sets of parameters studied, the intersection point height generally showed a broadly similar trend to decrease with increasing frequency, consistent with a prominent role of biomechanics. However, the best reproduction of the experimental results presented in [6] was obtained with a parameter set that enforced minimal control effort and penalized hip torque input more heavily than ankle torque. This result suggests that observations of the frequency-dependence of the intersection point height may quantify some details of the neural strategy that humans use in quiet standing in the sagittal plane.

This paper is organized as follows. The methods section summarizes the parameters used in the double inverted pendulum model, describes the linearization procedure, details the LQR controller design algorithm, and defines the weighting matrices tested. It also introduces the intersection point and outlines how it was computed. The results section presents key outcomes. The discussion interprets those results, especially the physiologically-plausible information supported by previous work that may be extracted from the frequency-dependent behavior of the intersection point height. The conclusion highlights the main outcomes and suggests how this study's methods may be used to quantify details of the controller humans use to balance under different conditions.

Methods

Simulation Setup

Double Inverted Pendulum Model

The double inverted pendulum model that was used to simulate a multi-segmented human body is illustrated in Fig. 1. It was the simplest model that could adequately portray the details of the phenomenon of interest: the frequency dependence of the intersection point height (see Appendix 1 for further justification).

The lumped model parameters summarized in Table 1 were based on the anthropometric distribution of male subjects in the sagittal plane [17] and the average height and weight of 71 kg and 1.75 m of the subjects from [6]. Any mass and length below the ankle was neglected, as the simulation assumed the ankle to be a pin joint. The center of mass positions are measured with respect to the ankle joint for link 1 and the hip

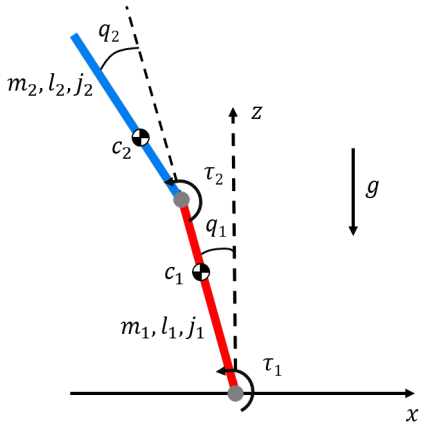

Figure 1 Double inverted pendulum model with angle (q_i) and torque (τ_i) conventions and parameter values for mass (m_i), length (l_i), center of mass (c_i), and moment of inertia about the center of mass (j_i). The direction of gravity (g) is also defined.

Table 1 Lumped Model Parameters

Symbol	Parameter (units)	Value	
		Link 1	**Link 2**
		Lower Body	Upper Body
m	**Mass** (kg)	26.30	42.88
l	**Length** (m)	0.867	0.851
c	**Center of mass** (m)	0.589	0.332
j	**Moment of inertia** (kgm^2)	1.400	2.227
g	**Gravitational acceleration** (m/s^2)	9.81	

joint for link 2. The moments of inertia were calculated about the center of mass of each link.

The equations of motion of the double inverted pendulum are

$$\mathbf{M}(\mathbf{q})\ddot{\mathbf{q}} + \mathbf{C}(\mathbf{q},\dot{\mathbf{q}})\dot{\mathbf{q}} + \mathbf{G}(\mathbf{q}) = \boldsymbol{\tau}, \quad (1)$$

where $\mathbf{M}(\mathbf{q}) \in \mathbb{R}^{2\times2}$ is the inertia matrix, $\mathbf{C}(\mathbf{q},\dot{\mathbf{q}}) \in \mathbb{R}^{2\times2}$ contains the Coriolis and centrifugal terms, $\mathbf{G}(\mathbf{q}) \in \mathbb{R}^{2\times1}$ are gravitational torques, and $\boldsymbol{\tau} = [\tau_1, \tau_2]^T \in \mathbb{R}^{2\times1}$ is the joint torque vector (see Appendix 2 for full symbolic inertia, centrifugal, and gravitational torque matrices). Generalized coordinates are $\mathbf{q} = [q_1, q_2]^T \in \mathbb{R}^{2\times1}$, where q_1 is the angle of the lower body link (link 1) measured from the upright position, and q_2 is the relative angle of the upper body link (link 2) measured from the lower body link position, as shown in Fig. 1. These variables represent the sagittal plane angular displacements of the ankle and hip joints respectively.

Defining state variables as $\mathbf{x} = [\mathbf{q}^T, \dot{\mathbf{q}}^T]^T$, (1) can be rewritten in state-determined form as

$$\dot{\mathbf{x}} = \begin{bmatrix} \dot{\mathbf{q}} \\ -\mathbf{M}(\mathbf{q})^{-1}(\mathbf{C}(\mathbf{q},\dot{\mathbf{q}})\dot{\mathbf{q}} + \mathbf{G}(\mathbf{q})) + \boldsymbol{\tau} \end{bmatrix}. \quad (2)$$

To simulate the internal perturbation that causes persistent sway in quiet standing humans, the joint torques were corrupted by actuation noise as

$$\boldsymbol{\tau} = \boldsymbol{\tau}_{\text{ctl}} + \mathbf{w}. \quad (3)$$

where $\boldsymbol{\tau}_{\text{ctl}} = [\tau_{\text{ctl},1}, \tau_{\text{ctl},2}]^T$ are the ankle and hip torques that stabilize the body. In this study, we assumed the noise $\mathbf{w} \in \mathbb{R}^{2\times1}$ was white, mutually uncorrelated, and followed a zero-mean Gaussian distribution with covariance matrix $E\{\mathbf{w}\mathbf{w}^T\} = diag\{\sigma_1^2, \sigma_2^2\}$.

The Linear Quadratic Regulator

This study used a nonlinear model with a linear controller. Hence, the nonlinear equations of motion (2) were first linearized about the upright balancing posture ($\mathbf{q}_* = \mathbf{0}$, $\dot{\mathbf{q}}_* = \mathbf{0}$, and $\boldsymbol{\tau}_* = \mathbf{0}$) as follows

$$\dot{\bar{\mathbf{x}}} = \mathbf{A}_{lin}\bar{\mathbf{x}} + \mathbf{B}_{lin}\bar{\boldsymbol{\tau}} + \mathbf{B}_{lin}\mathbf{w}, \quad (4)$$

where $\bar{\mathbf{x}} = \mathbf{x} - \mathbf{x}_*$, $\bar{\boldsymbol{\tau}} = \boldsymbol{\tau}_{\text{ctl}} - \boldsymbol{\tau}_*$, and $\mathbf{A}_{lin}$ and $\mathbf{B}_{lin}$ are linearized state and input matrices, respectively (see Appendix 3 for the linearized state-space matrices).

As normal human standing is evidently stable in the upright position, at least under normal conditions, the LQR method was chosen as it guarantees stable control. The LQR is an optimal linear state-feedback controller that minimizes the quadratic cost function

$$J = \int_0^\infty [\bar{\mathbf{x}}^T(t)\mathbf{Q}\bar{\mathbf{x}}(t) + \bar{\boldsymbol{\tau}}^T(t)\mathbf{R}\bar{\boldsymbol{\tau}}(t)]dt \quad (5)$$

to determine control torques

$$\boldsymbol{\tau}_{\text{ctl}} = -\mathbf{K}_{LQR}\mathbf{x}, \tag{6}$$

where $\mathbf{K}_{LQR}$ is the optimal control gain matrix found via the LQR procedure. The matrices $\mathbf{Q}$ and $\mathbf{R}$ in (5) weight the state and input deviations from zero in the cost function.

The LQR design procedure has a number of important features. It guarantees a stable closed-loop system[1], an attribute that is essential for the stabilization of an inherently unstable model. In addition, it has the interesting property that if the weighting on control effort is sufficiently large (corresponding to minimal control effort), the resulting closed-loop system has a well-defined behavior that is independent of the state weighting matrix $\mathbf{Q}$. To evaluate the working hypothesis that humans economize effort, the minimal-effort solution was of interest. Consequently, the choice of the state weighting matrix was not critical, and $\mathbf{Q} = I_4$, the identity matrix with dimension 4 was chosen, which equally penalized each state's deviation from equilibrium.

The input weighting matrix facilitated exploration of two important features of closed-loop control: the overall magnitude of the control effort, determined by the parameter α, and the relative magnitude of hip and ankle effort, determined by the parameter β. The designed LQR cost function for the control effort had a weighting matrix, $\mathbf{R}$, parameterized by α and β as

$$\mathbf{R} = \alpha \begin{bmatrix} \beta & 0 \\ 0 & 1/\beta \end{bmatrix}. \tag{7}$$

While α determines the relative cost between state deviation and control effort, β defines the relative penalty on the control exerted by the ankle and hip. When $\beta > 1$, the ankle torque is penalized more heavily than the hip, and vice versa when $\beta < 1$.

[1]To ensure stability, the state-space matrices $\mathbf{A}_{lin}$ and $\mathbf{B}_{lin}$ must be a controllable pair, the $\mathbf{Q}$ matrix must be symmetric positive semi-definite, and the $\mathbf{R}$ matrix must be symmetric positive definite.

Simulation Protocol

The simulation was conducted using semi-implicit Euler integration. The initial condition was set to $\mathbf{x}_0 = [0, 0, 0, 0]^T$. Replicating the experimental protocol of [6], each simulation was run for 50 seconds at 1000 Hz. All simulations were conducted in MATLAB 2020a (Mathworks, MA).

To observe the effect of altering the LQR controller parameters on the intersection point frequency-dependence, various parameters were tested. For brevity and clarity, only a sample of the tested parameters is presented in Table 2. The relative strength of the two noise sources was defined as $\sigma_r = \sigma_1/\sigma_2$. When α was varied, β and σ_r were kept constant at 0.3 and 0.9 respectively. When β was varied, α and σ_r were kept constant at 10^6 and 0.9, respectively. When σ_r was varied, α and β were kept constant at 10^6 and 0.3, respectively.

40 trials were conducted for each tested parameter set to enable statistical analysis of the simulated dependence of the intersection point height on frequency.

Intersection Point

Outputs of the Simulation

The horizontal and vertical components of the ground reaction force and the center of pressure were com-

Table 2 Tested Parameters

Parameter	Meaning	Value
α	Determines the relative cost between state deviation and controller	10^6
		10^4
		10^{-4}
β	Determines the relative cost between the ankle and hip control effort	2
		1
		0.3
σ_r	Determines the relative strength of ankle and hip noise	2
		0.9
		0.5

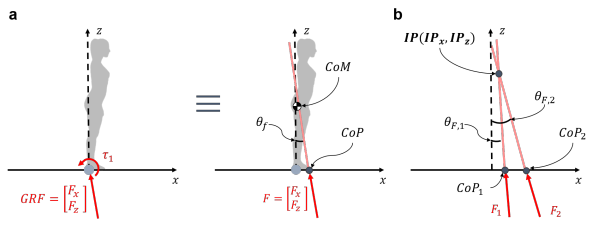

Figure 2 **a** The ankle torque, τ_1, and the ground reaction force, GRF, acting at the ankle joint can be represented by a net force, F, acting at the center of pressure, CoP. The GRF, made up of horizontal and vertical components, F_x and F_z, has an orientation θ_F. The center of mass, CoM, is also shown. **b** Two net force vectors, which are defined by their respective θ_F and CoP, intersect at the intersection point.

puted at every time step of the simulation to obtain the frequency-dependent behavior of the intersection point.

F_x and F_z, the horizontal and vertical components of the ground reaction force, were obtained as follows

$$F_x = m\ddot{r}_{CoM,x}, \quad F_z = m(\ddot{r}_{CoM,z} + g),$$

where $m = m_1 + m_2$ is the total mass of the body. $\ddot{\mathbf{r}}_{CoM} \in \mathbb{R}^{2\times 1}$ is the acceleration of the center of mass which was computed from

$$\ddot{\mathbf{r}}_{CoM} = \begin{bmatrix} \dot{\mathbf{J}}_{CoM} & \mathbf{J}_{CoM} \end{bmatrix} \dot{\mathbf{x}}. \tag{8}$$

$\mathbf{J}_{CoM} \in \mathbb{R}^{2\times 2}$ is the Jacobian of the center of mass with respect to the joint angles q_1 and q_2 (see Appendix 2 for the Jacobian expressed in terms of model parameters). The center of pressure, CoP, was then computed as

$$CoP = \frac{\tau_1}{F_z}.$$

Mechanics of the Intersection Point

The intersection point is a geometric representation of the relation between the ground reaction forces and the center of pressures in human subjects [6], as illustrated in Fig. 2.

Assuming subtle movements of the body and small variations in ground reaction forces, the orientation of the ground reaction force can be approximated as follows

$$-\frac{F_x}{F_z} = \tan\theta_F \approx \theta_F.$$

The intersection point of forces at two times can be obtained as

$$IP_x = \frac{\theta_{F,1}CoP_2 - \theta_{F,2}CoP_1}{\theta_{F,1} - \theta_{F,2}},$$
$$IP_z = \frac{CoP_1 - CoP_2}{\theta_{F,1} - \theta_{F,2}}.$$

Again, assuming small variation between the forces,

$$\theta_{F,2} \approx \theta_{F,1} + d\theta_F, \quad COP_2 \approx CoP_1 + dCoP.$$

Then, the lower-order component of the intersection point can be obtained as

$$IP_x = \frac{CoPd\theta_F - \theta_F dCoP}{d\theta_F}, \quad IP_z = \frac{dCoP}{d\theta_F}. \tag{9}$$

Frequency-Dependence of the Intersection Point

A Hamming window[2] with the length of the entire data set was first applied to both θ_F and CoP signals. θ_F and CoP signals were then bandpass-filtered (zero-lag, 2nd-order Butterworth) in bands of 0.2 Hz centered on frequencies from 0.5 to 7.9 Hz (38 non-overlapping bands). Finally, the principal eigenvector of the best-fit covariance matrix of θ_F plotted against CoP (both signals detrended to have zero-mean) was extracted. Its slope is equivalent to the inverse of the intersection point, as illustrated in Fig. 3, because rearranging (9) results in

$$d\theta_F = \frac{1}{IP_z} dCoP. \tag{10}$$

[2] The Hamming window reduces side lobes, or local maxima in the frequency domain, that arise when transforming finite-length time-domain data into the frequency domain.

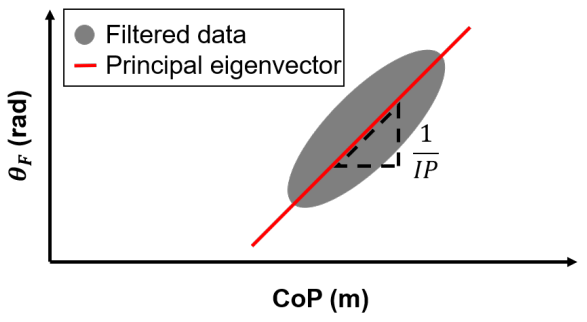

Figure 3 An illustration of the relation between θ_F and CoP for one theoretical simulation trial of any given parameter set. The data was processed by filtering the CoP and θ_F signals using a 2nd-order bandpass filter with a 0.2 Hz wide frequency band. The principal eigenvector of the covariance matrix of the filtered data was extracted. The intersection point (IP) was computed as the inverse of the slope of the principal eigenvector. Note that the time series of the data was approximated as an ellipse in this schematic illustration.

Comparison of Simulation and Human Experimental Results

When determining the goodness of fit across different model parameter conditions, the average difference of the simulated data compared to the human subject data from [6] was computed by

$$\text{average difference} = \frac{\sum_{i=1}^{N} \text{Human Data}_i - \text{Simulation Data}_i}{N}, \quad i = 1, 2, ...N.$$

where Human Data_i is the median of the intersection point height as a fraction of the center of mass height reported in [6] at each frequency band; Simulation Data_i is the average intersection point height as a fraction of the center of mass height across 40 trials of the simulation data in a given frequency band; N is the number of frequency bands for which the difference in the data was computed. Because balance is characterized by only small motions, a constant center of mass height was assumed.

In the data reported in [6], the intersection point was higher than the center of mass at lower frequencies and approached an asymptote approximately exponentially at higher frequencies, crossing the center of mass height in a specific frequency range (1.2 – 2.6 Hz; see Fig. 4a). To identify the onset of the asymptote, the human data was fit to an exponential function. The best-fit decay constant was $T \cong 1$ Hz. Assuming the curve reached its asymptote at frequency $\cong 3T$, the asymptote started at 3 Hz. The difference between the simulated and experimental asymptote was evaluated at frequencies 3 – 8 Hz, $N = 25$. To evaluate the effect of different controller parameters in the frequency range in which the experimentally observed intersection point height was not statistically different from the center of mass height, the average difference between simulation and human data was evaluated over 1.2 – 2.6 Hz, and $N = 7$. One-sample t-tests were used to evaluate the difference between the center of mass height and the simulated mean intersection point height. The 95% confidence interval of the mean of the difference was computed as well.

Results

The simulated center of mass height did not deviate far from 0.97 m, the height of the center of mass when the simulated system was perfectly upright, justifying the assumption of small angular displacement used to linearize the equations of motion and approximate the intersection point height. In what follows, the center of mass height was assumed to be constant.

Best-Fit Model Parameter Set

The simulated frequency-dependent intersection point response for the parameter set, $\alpha = 10^6$, $\beta = 0.3$, $\sigma_r = 0.9$, best matched the human subject data from [6] as shown in Fig. 4. Both simulation and human experimental results show that the intersection point height crossed the center of mass height in similar fre-

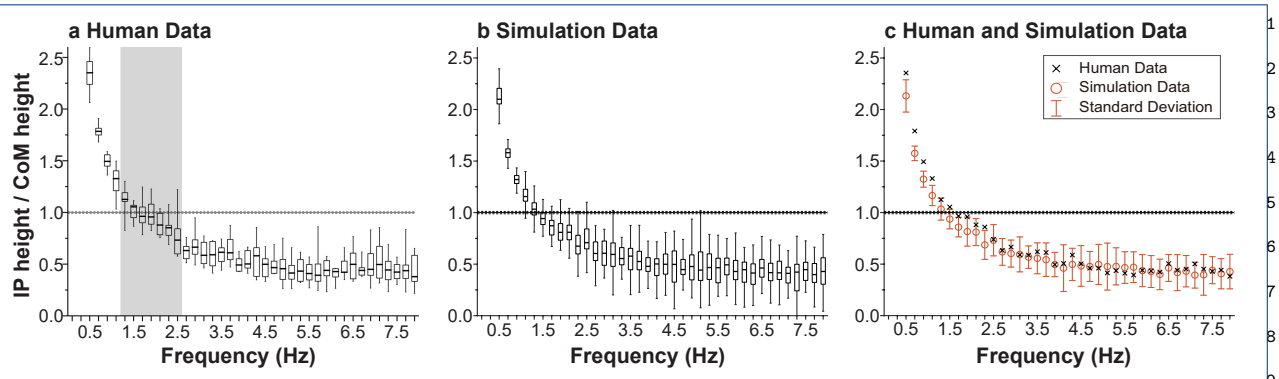

Figure 4 Comparison of the intersection point's frequency-dependence from (**a**) human experimental data (reproduced from [6] with permission) and (**b**) simulation data. The mean of the simulation data overlaid on the median of the human data from [6] is shown in (**c**). The parameters used in the simulation were $\alpha = 10^6$, $\beta = 0.3$, $\sigma_r = 0.9$. The height at which the intersection point crossed the center of mass is indicated with a dashed line. Within the frequency band from 1.2 – 2.6 Hz for the human data, there was no significant difference (with 95% confidence) between the mean of the intersection point height and the center of mass height. This frequency band is marked by the shaded region. In the simulation data, all frequency bands showed a significant difference between the mean of the intersection point height and the center of mass height. The high-frequency asymptote (3 – 8 Hz range) of the intersection point is 0.479 ± 0.028 and 0.468 ± 0.021 for the human and simulation data, respectively (with 95% confidence).

quency bands (1.2 – 2.6 Hz) and had similar high-frequency asymptotes. The difference compared to human data for this parameter set was 0.101 ± 0.040 in the 1.2 – 2.6 Hz range and 0.011 ± 0.019 in the 3 – 8 Hz range (both within the 95% confidence interval).

Varying Model Parameters

Varying the simulation parameters affected both the frequency at which the intersection-point crossed the center-of-mass height and the high-frequency asymptote. The effect of changing parameter values is summarized in Table 2 and presented in Fig. 5. The differences between simulation data and human data for certain parameter sets are also shown in Fig. 5.

Effect of α

As shown in Fig. 5a, when α, the weighting of control effort relative to state deviation, was increased, the intersection point crossed the center of mass at lower frequencies. For example, when α was varied from 10^4 to 10^6, the frequency at which the intersection point crossed over the center of mass moved from 3.9 Hz to 1.5 Hz. When α was relatively large ($\alpha > 10^4$), there was little effect of varying its value on the difference between human and simulation data for different model parameter sets, as shown in Fig. 5d and 5e.

Effect of β

As shown in Fig. 5b, when β was decreased, i.e. when hip control was penalized more than ankle control, the intersection point crossed the center of mass at higher frequencies. For example, when β was varied from 1 to 0.3, the frequency at which the intersection point crossed over the center of mass moved from 1.1 Hz to 1.5 Hz. In Fig. 5d, $\beta = 0.2$ was shown to be the parameter with the smallest difference (0.024) in the 1.2-2.6 Hz range when $\alpha = 10^6$. However, both the selection of $\beta = 0.2$ and $\beta = 0.1$ sacrificed the high-frequency fit, increasing the absolute value of the difference in the 3 – 8 Hz range by 0.102 and 0.292, respectively, compared to $\beta = 0.3$ when $\alpha = 10^6$. As β deviated from $\beta = 0.3$, the absolute value of the difference in the 1.2 – 2.6 Hz range increased by 0.181 when $\beta = 1$ and $\alpha = 10^6$.

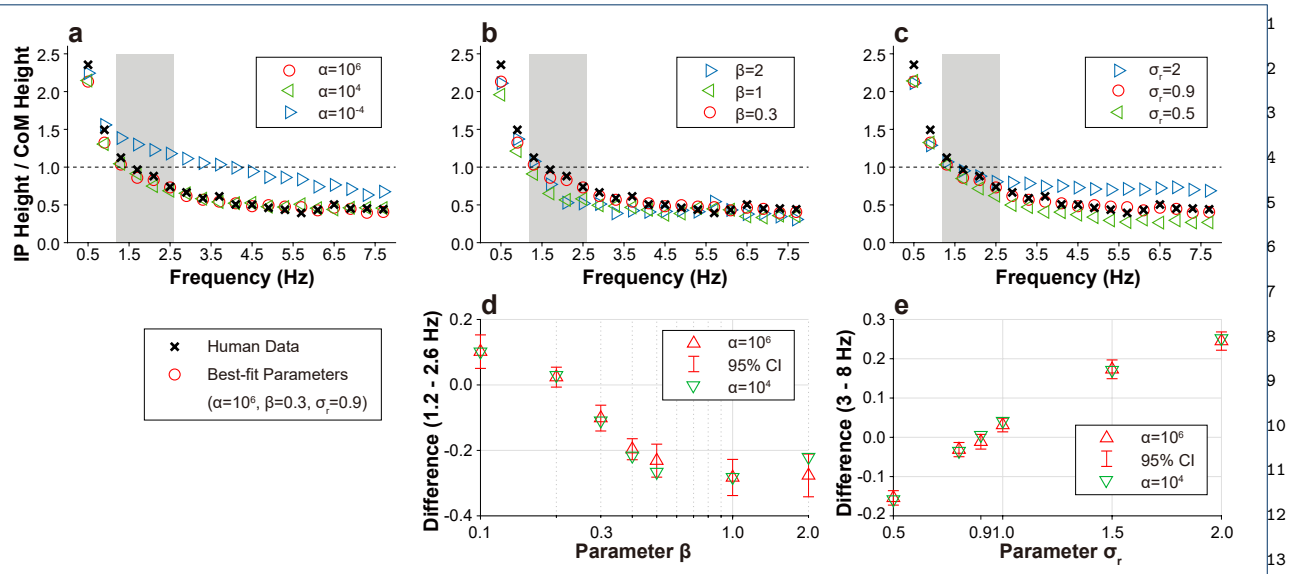

Figure 5 The effect of varying parameter values on the frequency-dependence of the intersection point. Each model parameter was varied with respect to the "best-fit" parameter set that closely resembled human subject data observed in [6] ($\alpha = 10^6$, $\beta = 0.3$, $\sigma_r = 0.9$). The height of the center of mass is indicated by a dashed line. The shaded region, based on human experiments, indicates the frequency band in which the mean of the intersection point height was not significantly different from the center of mass height in [6]. **a** The parameter α determined the cost of the overall magnitude of the control effort relative to state deviation from equilibrium. When varying α, the other parameters were set to $\beta = 0.3$ and $\sigma_r = 0.9$. **b** The parameter β determined the relative cost of ankle and hip torque. When $\beta > 1$, there was more penalty on ankle torque. When varying β, the other parameters were set to $\alpha = 10^6$ and $\sigma_r = 0.9$. **c** The parameter σ_r determined the relative strength of noise in the ankle and the hip. When $\sigma_r > 1$, ankle noise was greater than hip noise. When varying σ_r, the other parameters were set to $\alpha = 10^6$ and $\beta = 0.3$. **d** The difference of the intersection point in the 1.2 – 2.6 Hz frequency range of the simulated data compared to the human subject data [6] with respect to β. The parameter σ_r was kept at 0.9. **e** The difference of the intersection point in the 3 – 8 Hz frequency range of the simulated data compared to the human subject data [6] with respect to σ_r. The parameter β was kept at 0.3. In both cases, the effect of varying α is also shown. The error bars indicate the 95% confidence interval of the mean of difference when $\alpha = 10^6$.

Effect of σ_r

Adjusting σ_r shifted the high frequency asymptote (3 – 8 Hz range) of the intersection point, as shown in Fig. 5c. When compared to the best-fit height of the intersection point at high frequencies, the asymptote was 55% higher when $\sigma_r = 2$ (more noise in the ankle) and 30% lower when $\sigma_r = 0.5$ (more noise in the hip). In Fig. 5e, $\sigma_r = 0.9$ is shown to be the best-fit parameter with the smallest difference value, at -0.011 when $\alpha = 10^6$. As σ_r deviated from the best-fit value (both increasing/decreasing σ_r), the difference increased to 0.245 when $\sigma_r = 2$ and to -0.154 when $\sigma_r = 0.5$, when $\alpha = 10^6$.

Discussion

In this paper we analyzed a deliberately-simplified model of quiet standing with a series of stabilizing linear controllers using different parameter values to better understand the origin of the frequency-dependent intersection point reported by Gruben and colleagues [6]. Despite the existence of biomechanical constraints that limit the admissible combinations of translational and rotational accelerations and the center of pressure range available to a balancing human [12,13], the ground reaction force options to comply with these constraints are infinite [8,18]. By extension, we should not expect mechanics alone to determine the intersection point's frequency dependence. When Gruben

and colleagues [6] analyzed the frequency dependence of the intersection point, they observed a consistent trend across multiple subjects and suggested that this consistency was a signature of a neural controller employed by humans during balance. By simulating stable controllers of a simple model, this study aimed to clarify the roles that biomechanical constraints and neural control strategies might play in producing this behavior. The observed decrease in intersection point height with frequency appears to reflect a biomechanical constraint, while specific variations in the shapes of the curves resulted from different controller parameters and actuation noise ratios.

Neural Control Strategy or Biomechanical Constraint?

The results of our simulations replicated the frequency dependence of the intersection point reported for human standing in the sagittal plane: the intersection point was above the center of mass at low frequencies and below the center of mass at high frequencies. For obvious reasons, this study only considered stabilizing controllers. That was our main reason for using the LQR design procedure, which results exclusively in stable controllers, at least for the small deviations from upright posture that are typically observed. Importantly, this stabilizing controller was able to replicate the general variation of intersection point height with frequency for a wide range of model parameters and performance criteria.

That fact alone is likely due to the biomechanical constraints that the human body imposes on the task. For small deviations from upright posture, the double inverted pendulum has two modes of behavior from which all other motions may be composed: a mode in which ankle and hip move in phase, and a mode in which ankle and hip move anti-phase. Mechanics dictates that the in-phase mode must occur at a lower frequency than the anti-phase mode. Ankle and hip torques that restore upright posture after small deviations must be in phase for the lower-frequency mode (the so-called "ankle strategy") [19–21]. This mode would place the intersection point above the center of mass. Conversely, ankle and hip torques that restore upright posture must be out of phase for the higher-frequency mode (the so-called "hip strategy"), which would place the intersection point below the center of mass.

Therefore, somewhere between the low-frequency and high-frequency regimes, the intersection point must cross from above to below the center of mass. This crossing point is not specified by biomechanics. Similarly, biomechanics does not dictate the asymptote to which the intersection point height converges at high frequencies. In fact, the frequency at which the intersection point height crossed that of the center of mass and the intersection point's high frequency asymptote both varied across tested parameters. In summary, only a small set of parameters could replicate human behavior. Therefore, we conclude that the details of the profile of intersection point height with frequency reflect a neural control strategy used by humans during quiet stance.

Physiologically-Plausible Best-Fit Parameters

In particular, one set of model parameters, $\alpha = 10^6, \beta = 0.3, \sigma_r = 0.9$, closely reproduced the behavior that was observed in human experiments. This parameter set yielded the simulated intersection point frequency response with the smallest difference from human data over the entire frequency range of interest. Interpreting the influence of each model parameter that was varied to obtain this best-fit result may provide insight.

First, changing α affected the frequency at which the intersection point crossed the center of mass. This parameter dictates the relative cost of state deviations from zero (angles and angular velocities) and control input (torques) as shown in (7). The parameter value

that yielded the best-fit result compared to human data, $\alpha = 10^6$, penalized the control input the most out of tested α values. Remarkably, the resulting controller used the least control effort compatible with maintaining upright balance. In the LQR procedure, when α is large, the unstable open-loop poles maintain their absolute values but migrate to stable closed-loop poles. In other words, this parameter set places stable closed-loop poles at the mirror images of the unstable open-loop poles and is termed the "minimal control" solution. Since selecting $\alpha = 10^6$ resulted in this pole movement, the best-fit solution was a result of minimal stabilizing control. Therefore, a double inverted pendulum model with minimal control effort provides an explanation for the frequency-dependent intersection point response observed in humans. This result implies that humans may minimize control effort during quiet standing, which is consistent with the observation found in a previous study that the nervous system does not produce more control effort than what is necessary to stabilize upright balance [22]. In addition, Fig. 5d and 5e show that there was little effect of changing α when it was selected to be sufficiently large ($\alpha > 10^4$), leaving only two parameters, β and σ_r, to be adjusted to search for the best-fit solution.

Second, varying β also affected the frequency at which the intersection point height crossed that of the center of mass. Unlike α, however, the best-fit β parameter was not at the extreme range of the tested parameter set. Instead, the condition that best describes human data, $\beta = 0.3$, is one that penalizes hip control more than ankle control. That is, the system is more likely to use the ankle to maintain upright posture. When β deviated from this best-fit value, the average difference increased, indicating that the relative weighting between the ankle and the hip was determinative and potentially informative. In the study by Gruben and colleagues [6], human subjects were tasked with quiet standing, which does not involve any major external perturbations and is commonly achieved with minimal hip flexion (the "ankle strategy") [13, 19–21]. The best-fit solution also penalized the use of the hip, suggesting that simulation outcomes have the potential to inform us of human neural control strategy. Note that although $\beta = 0.2$ yielded a smaller difference between the simulation and human data than $\beta = 0.3$ in the 1.2-2.6 Hz range as shown in Fig. 5d, it sacrificed the overall fit as the absolute difference in the $3 - 8$ Hz range increased by 0.102; thus, $\beta = 0.3$ provided a better overall fit.

Third, altering the relative noise magnitude in the ankle and the hip torques shifted the high-frequency asymptote of the intersection point height. This result is predicted by the analysis presented in Appendix 4, where two extremes, zero noise in the ankle ($\sigma_r = 0$) and the hip ($\sigma_r = \infty$), provide the upper and lower bound of the high frequency asymptote. Similar to β, the best-fit relative noise magnitude was not at the extreme of the range for the tested parameter set. Specifically, the simulation result most similar to human experimental data had a $0.9 : 1$ ankle-to-hip noise ratio, and any deviation from this ratio resulted in a larger absolute value of the average difference. Therefore, the ratio of noise is determinative and potentially informative. It has been reported that for tasks that require isometric force production, such as quiet standing, force variability scales linearly with mean force production [23]. Although the best-fit β in our results indicates that the ankle is being relied on more for torque production, the best-fit noise ratio prescribes a slightly lower noise in the ankle joint. The discrepancy between our work and previous work should be investigated in future studies, possibly by adding other noise sources to the system such as sensory noise.

Limitations

The simulations conducted in this study assumed simple mechanics. The joint torques in the model are net joint torques that summarize the contributions of various elements, from passive muscle properties to complex neural control. Known features of neuromuscular physiology such as muscle mechanical impedance, neural transmission delay, or sensory noise were omitted. While these features are unquestionably present, our goal was to identify the simplest model competent to reproduce experimental observations. Despite their acknowledged limitations, our simulations were able to articulate subtle differences between control parameters that influence intersection point frequency-dependence. Nevertheless, including those neurophysiological features might yield further insight; that is deferred to future work.

The use of a double-inverted pendulum model (2 DOF) was necessitated by the fact that a single-inverted pendulum model (1 DOF) proved to be unable to reproduce experimental observations. As shown in Appendix 1, if the human body is modeled as a single-DOF inverted pendulum, no matter what controller is implemented, the intersection point height converges above the center of mass at high frequencies. Although the single-inverted pendulum model has been used to model quiet human standing [1,14,24–26], it cannot provide a competent description of the experimental data observed by Gruben and colleagues [6], where the intersection point height converged below the center of mass at high frequencies. The intersection point frequency trend observed in humans requires multi-segment mechanics.

The finding that a single-segment model cannot adequately describe human quiet standing is consistent with recent literature. For example, Loram and Lakie [15] observed that human ankle stiffness (estimated from human subject experiments) was insufficient to stabilize the body when it was modeled as a single inverted pendulum and proposed a widely-accepted conclusion that intrinsic mechanical impedance is inadequate to maintain balance. However, Rozendaal and van Soest [27] reported that the ankle stiffness required for stabilization was not as large as predicted by Loram and Lakie [15] when the body was modeled as a double-inverted pendulum, suggesting that the data may have been misinterpreted due to an oversimplified model.

Why no more than two degrees of freedom? It is patently obvious that the standing human body has many more degrees of freedom. However, although adding a knee joint [28] or multiple segments of the spine might more accurately replicate human biomechanics, it is not clear that this would improve the insight to be gleaned from experimental observations. In fact, as shown in Appendix 4, the two-segment model yields a high-frequency asymptote for the intersection point height that must lie between zero (corresponding to zero noise at the ankle) and below the center of mass height (corresponding to zero noise at the hip). These two extremes bracket the experimental observations reported by Gruben and colleagues [6]. Thus the two-segment model used in this study was the simplest that could competently reproduce the experimental results observed by Gruben and colleagues [6]. Other balance scenarios (e.g. the use of secondary supports such as canes) may require the inclusion of more degrees of freedom.

This study assumed a linear full-state feedback controller with a constant gain matrix (i.e. proportional feedback of angle and angular velocity) even though the central nervous system is comprised of many nonlinear neural elements. This decision was motivated by the observation that the body makes small motions about upright posture. That justified using a model

that was linearized about upright posture to obtain feedback controller gains.

We must emphasize that this study does not presume to conclude that the neural balance strategy is a linear controller optimizing a quadratic performance criterion. The LQR design procedure was simply a tool to generate stabilizing controllers for an inherently unstable system while simultaneously analyzing the influence of factors like the cost of control on balance performance.

Quantitative Analysis Provides Insight into Human Neural Control Strategy

Having established the effect of the controller on the frequency-dependence of the intersection point height, a question that may be raised is whether the intersection point is a target of control. In this study, the signal fed back to the controller was the state error (joint angles and angular velocities) rather than the intersection point. Even so, this study was able to replicate the frequency dependence of the intersection point found in humans. Therefore, consistent with the findings of Blickhan and colleagues [29], it appears that the intersection point may be an emergent consequence of stabilization rather than a variable explicitly regulated by the controller. However, further experimentation would be required to test this hypothesis.

The two-segment model employed in this study permits interpretation of the results with respect to the "ankle strategy" and the "hip strategy". The double-inverted pendulum has two modes corresponding to the aforementioned strategies, and the general behavior is a weighted sum of these modes. The two postural strategies were originally thought to be distinct [20]; however, it is now commonly believed that the two produce a continuum of postural control strategies [21, 30]. The results of the simulation study reported here are consistent. The intersection point frequency-dependence demonstrates that humans use a combination of hip and ankle strategies to balance. The combination is required presumably because neuromuscular control appears stochastic with a broad frequency spectrum. To account for fluctuations from upright posture, our model included additive white noise processes (with theoretically infinite bandwidth); its success indicates that this is a serviceable description of neural control, at least in this context. When the intersection point is above the center of mass at low frequencies, the ankle strategy dominates, and when it is below the center of mass at high frequencies the hip strategy dominates. Though the details of the frequency-dependent intersection point curve varied when different controllers were tested, this general feature did not change, indicating that it is a consequence of biomechanics.

The main contribution of this work is that it successfully deployed a mathematical model with an optimal control scheme to quantitatively account for the human experimental results reported by Gruben and colleagues [6]. Its success implies that it may elucidate the neural control of quiet standing. To conduct this quantitative analysis, the model parameters were systematically varied such that the simulated intersection point frequency-dependent response closely replicated human data. First, the parameter that weights the relative cost of the control input, α, was set to ensure minimal control ($\alpha > 10^4$). This design choice effectively reduced the number of parameters to tune to two (β and σ_r) as the resulting intersection point frequency-dependence did not vary as long as α was sufficiently large. Then, the noise ratio, σ_r, was adjusted to produce best fit at high frequencies while setting $\beta = 1$. Lastly, the parameter that weights the relative cost of the hip and ankle joint torque inputs, β, was varied to produce best fit in the frequency range where the intersection point height was approximately equivalent to the center of mass height. At the same

time, it was ensured that the asymptotic behavior and the fit at high frequencies were maintained. Given the long transmission delays in the neural system, stability requires any continuous feedback loop gain to be effectively zero at high frequencies. However, muscle mechanical impedance is not limited in this way; it can respond essentially instantaneously. Control in the high frequency range is therefore not likely to depend on neural feedback (defined by α and β), but instead on neuromuscular impedance and noise (defined by σ_r). Hence, the noise ratio, σ_r, was adjusted to fit the high frequency range before fitting the low frequency range with β.

These specific parameter values may serve to quantify how humans maintain balance in the sagittal plane. In future studies, model parameter adjustments may serve as a powerful tool to match the intersection point simulation data with human experimental data to draw quantitative conclusions about neural strategies in a variety of other conditions.

Conclusion

This study compared the frequency dependence of the intersection point height resulting from simulations against outcomes from human experiments in an effort to quantify neural control and its interaction with biomechanics. Not only does this study confirm the obvious role of control in human balance, it also identifies quantitative measures that may lead to a better understanding of the costs that humans weigh when selecting a balance strategy. This work introduced a systematic method by which human data can be reproduced by selecting specific, quantitative control and noise parameters. This method can be extended to different experimental conditions that may yield different intersection point behavior and best-fit controller parameters. The frequency-dependence of the intersection point should be measured for varying conditions such as sagittal and frontal plane balance, with and without assistive devices like canes, or in aged and impaired populations. The measured data can then be compared against simulation data to identify the difference in controller characteristics employed by humans in different conditions.

Appendix 1: Intersection Point of the Single Inverted Pendulum

The observed intersection point behavior at high frequencies cannot be reproduced by a single inverted pendulum model, which is widely used to model human quiet balancing. Consider a single inverted pendulum model with mass m, center of mass position from the pivot c, moment of inertia about ankle pivot j', and gravitational acceleration g. Ankle torque τ is the only actuator. The governing equation of motion is

$$j'\ddot{q} - mgc\sin q = \tau = \tau_{\text{ctl}} + w, \tag{11}$$

where q is the angular displacement of the ankle joint with respect to the upright equilibrium posture, τ_{ctl} is the torque commanded by the central nervous system, and w is the actuation noise. For small motion typical of unperturbed balance, linearization of (11) is well justified:

$$j'\ddot{q} - mgcq = \tau.$$

Likewise, the two outputs of interest are linearized. As introduced in (10), the intersection point is defined in terms of the orientation of the force, θ_F, and the center of pressure, CoP. Each are defined as

$$\theta_F = -\frac{F_x}{F_z} \approx \frac{mc\ddot{q}}{mg} = \frac{c}{g}\ddot{q}, \quad CoP = \frac{\tau}{F_z} \approx \frac{\tau}{mg}.$$

One can take the Laplace transform of the outputs and obtain

$$\Theta_F(s) = \frac{c}{g}s^2Q(s), \quad COP(s) = (\frac{j'}{mg}s^2 - c)Q(s).$$

where s is a complex variable, $Q(s)$, $\Theta_F(s)$, and $COP(s)$ are the Laplace transformations of q, θ_F, and CoP, respectively. Denote $H(s) = Q(s)/W(s)$, the transfer function from input noise to output motion, where $W(s)$ is the Laplace transformation of w. Note that at high frequency Ω, the two outputs have exactly the same phase because both of them simply add $-\pi$ to the phase of $H(i\Omega)$ (consider $s = i\Omega$ where $i^2 = -1$ and $\Omega \to \infty$). Then the variation of two output variables will be perfectly linear at high frequencies and the intersection point at each frequency can be simply determined from the ratio of magnitudes of the two outputs:

$$IP_z(\Omega) = \frac{|COP(i\Omega)|}{|\Theta_F(i\Omega)|} = \frac{\frac{j'}{mg}\Omega^2 + c}{\frac{c}{g}\Omega^2} = \frac{j'\Omega^2 + mgc}{mc\Omega^2}.$$

As $\Omega \to \infty$,

$$IP_z(\Omega) \to \frac{j'}{mc} = \frac{j + mc^2}{mc^2} = c + \frac{j}{mc} > c.$$

In other words, the intersection point height is always greater than the center of mass height. Note that the centroidal moment of inertia is $j = j' - mc^2$. Therefore, the intersection point height must be greater than the center of mass height; in other words, the single rigid-body inverted pendulum model cannot explain an intersection point below the center of mass at high frequencies.

Appendix 2: Nonlinear Model Equations

The equations of motion of the double inverted pendulum are expressed in (1). Note that the choice of generalized coordinates, q_1, q_2, are consistent with the generalized forces (torques) that are applied. The following are each of the matrices in terms of the inertial parameters in Table 1. j_1' and j_2' denote moment of inertia taken about ankle and hip joint pivots, respectively. l_{c1} is the distance from the ankle joint pivot to the center of mass of link 1, and l_{c2} is the distance from the hip joint pivot to the center of mass of link 2. $\cos(q_i)$ and $\sin(q_i)$ are replaced with c_i and s_i, respectively. Setting $\theta_2 = q_1 + q_2$, $\cos(\theta_2)$ and $\sin(\theta_2)$ are replaced with c_{θ_2} and s_{θ_2}, respectively.

$$\mathbf{M}(\mathbf{q}) = \begin{bmatrix} j_1' + j_2' + m_2(l_1^2 + 2l_1 l_{c2} c_2) & j_2' + m_2 l_1 l_{c2} c_2 \\ j_2' + m_2 l_1 l_{c2} c_2 & j_2' \end{bmatrix}$$

$$\mathbf{C}(\mathbf{q}, \dot{\mathbf{q}}) = m_2 l_1 l_{c2} s_2 \begin{bmatrix} -2\dot{q}_2 & -\dot{q}_2 \\ \dot{q}_1 & 0 \end{bmatrix}$$

$$\mathbf{G}(\mathbf{q}) = -g \begin{bmatrix} m_1 l_{c1} s_1 + m_2(l_1 s_1 + l_{c2} s_{\theta_2}) \\ m_2 l_{c2} s_{\theta_2} \end{bmatrix}$$

The ground reaction forces are characterized by the motion of the center of mass. To obtain the acceleration of the center of mass as shown in (8), its Jacobian and the derivative of its Jacobian are given as follows

$$\mathbf{J}_{CoM,1} = \begin{bmatrix} M_1 l_{c1} c_1 + M_2(l_1 c_1 + l_{c2} c_{\theta_2}) \\ M_1 l_{c1} s_1 + M_2(l_1 s_1 + l_{c2} s_{\theta_2}) \end{bmatrix}$$

$$\mathbf{J}_{CoM,2} = \begin{bmatrix} M_2 l_{c2} c_{\theta_2} \\ M_2 l_{c2} s_{\theta_2} \end{bmatrix},$$

where

$$\mathbf{J}_{CoM} = -\begin{bmatrix} \mathbf{J}_{CoM,1} & \mathbf{J}_{CoM,2} \end{bmatrix},$$

and

$$\dot{J}_{CoM,(1,1)} = M_1 l_{c1} \dot{q}_1 s_1 + M_2(l_1 \dot{q}_1 s_1 + l_{c2} \dot{\theta}_2 s_{\theta_2})$$
$$\dot{J}_{CoM,(1,2)} = M_2 l_{c2} \dot{\theta}_2 s_{\theta_2}$$
$$\dot{J}_{CoM,(2,1)} = -M_1 l_{c1} \dot{q}_1 c_1 - M_2(l_1 \dot{q}_1 c_1 + l_{c2} \dot{\theta}_2 c_{\theta_2})$$
$$\dot{J}_{CoM,(2,2)} = -M_2 l_{c2} \dot{\theta}_2 c_{\theta_2}$$

where

$$\dot{\mathbf{J}}_{CoM} = \begin{bmatrix} \dot{J}_{CoM,(1,1)} & \dot{J}_{CoM,(1,2)} \\ \dot{J}_{CoM,(2,1)} & \dot{J}_{CoM,(2,2)} \end{bmatrix},$$

and $M_1 = \frac{m_1}{m_1+m_2}$ and $M_2 = \frac{m_2}{m_1+m_2}$.

Appendix 3: Linearized State-Space Matrices

Linearizing the equations of motion about the stable upright position, we are left with (4). The state-space matrices are

$$\mathbf{A}_{lin} = \begin{bmatrix} \mathbf{0} & \mathbf{I} \\ \mathbf{M}^{-1}\frac{\partial \mathbf{G}}{\partial \mathbf{q}} & \mathbf{0} \end{bmatrix}_{\mathbf{x}=\mathbf{x}^*,\boldsymbol{\tau}=\boldsymbol{\tau}^*}$$

$$\mathbf{B}_{lin} = \begin{bmatrix} \mathbf{0} \\ \mathbf{M}^{-1}\mathbf{B} \end{bmatrix}_{\mathbf{x}=\mathbf{x}^*,\boldsymbol{\tau}=\boldsymbol{\tau}^*}$$

where

$$\left.\frac{\partial \mathbf{G}}{\partial \mathbf{q}}\right|_{\mathbf{x}=\mathbf{x}^*} = -g \begin{bmatrix} m_1 l_{c1} + m_2(l_1 + l_{c2}) & m_2 l_{c2} \\ m_2 l_{c2} & m_2 l_{c2} \end{bmatrix}$$

and $\mathbf{B} = \mathbf{I}_2$.

Appendix 4: Intersection Point of the Linearized Double Inverted Pendulum

We can linearize the output equations in conjunction with the linearized equations of motion in (4). Noting that $\theta_F \approx -F_x/F_z, CoP = \tau_1/F_z$, let us consider two outputs $\mathbf{y} = [y_1, y_2]^T$: $y_1 = -F_x = -m\ddot{r}_{CoM,x}$, $y_2 = \tau_1$. From (8), $y_1 = -m[1,0]\ddot{\mathbf{r}}_{CoM} = -m[1,0][\dot{\mathbf{J}}_{CoM}, \mathbf{J}_{CoM}]\dot{\mathbf{x}} \triangleq \mathbf{J}_{y_1}\dot{\mathbf{x}}$. Then, linearized output equations can be obtained as

$$\mathbf{y} = \mathbf{C}\mathbf{x} + \mathbf{D}\boldsymbol{\tau} = \begin{bmatrix} \mathbf{C}_1 \\ \mathbf{C}_2 \end{bmatrix}\mathbf{x} + \begin{bmatrix} \mathbf{D}_1 \\ \mathbf{D}_2 \end{bmatrix}\boldsymbol{\tau},$$

where $\mathbf{C}_1 = \mathbf{J}_{y_1}\mathbf{A}_{lin}, \mathbf{D}_1 = \mathbf{J}_{y_1}\mathbf{B}_{lin}$, evaluated at $(\mathbf{x}, \boldsymbol{\tau}) = (\mathbf{x}^*, \boldsymbol{\tau}^*)$, and $\mathbf{C}_2 = \mathbf{0}, \mathbf{D}_2 = [1, 0]$. With controller $\boldsymbol{\tau} = -\mathbf{K}\mathbf{x} + \mathbf{w}$ as in (3) and (6), the closed-loop linear system can be constructed as

$$\begin{cases} \dot{\mathbf{x}} = (\mathbf{A_{lin}} - \mathbf{B_{lin}}\mathbf{K})\mathbf{x} + \mathbf{B_{lin}}\mathbf{w} = \mathbf{A}_{\mathrm{cl}}\mathbf{x} + \mathbf{B_{lin}}\mathbf{w} \\ y_1 = (\mathbf{C}_1 - \mathbf{D}_1\mathbf{K})\mathbf{x} + \mathbf{D}_1\mathbf{w} = \mathbf{C}_{\mathrm{cl},1}\mathbf{x} + \mathbf{D}_1\mathbf{w} \\ y_2 = (\mathbf{C}_2 - \mathbf{D}_2\mathbf{K})\mathbf{x} + \mathbf{D}_2\mathbf{w} = \mathbf{C}_{\mathrm{cl},2}\mathbf{x} + \mathbf{D}_2\mathbf{w}. \end{cases} \quad (12)$$

The multi-input, multi-output (MIMO) transfer function can be obtained

$$\mathbf{Y}(s) = \mathbf{H}(s)\mathbf{W}(s), \quad \mathbf{H}(s) = \begin{bmatrix} H_{11}(s) & H_{12}(s) \\ H_{21}(s) & H_{22}(s) \end{bmatrix}$$

where $\mathbf{Y}(s)$ and $\mathbf{W}(s)$ are the Laplace transformations of $\mathbf{y}$ and $\mathbf{w}$, respectively. The intersection point at each frequency can be obtained by bandpass-filtering signals, then conducting principal component analysis to find the principal eigenvector of the best-fit covariance matrix of $y_1(t)$ and $y_2(t)$. The intersection point is defined as the inverse of the slope of the principal eigenvector. If $y_1(t)$ and $y_2(t)$ are harmonic, this procedure is equivalent to finding the slope of the major axis of an ellipsoid that the two signals form.

Assuming two harmonic signals $y_i(t)$ with magnitude ν_i and phase ϕ_i at frequency Ω,

$$y_1(t) = \nu_1 \sin(\Omega t + \phi_1), \quad y_2(t) = \nu_2 \sin(\Omega t + \phi_2),$$

an implicit formula for the ellipsoid can be written in a quadratic form,

$$\sin^2\phi = [y_2, y_1] \begin{bmatrix} \frac{1}{\nu_2^2} & -\frac{\cos\phi}{\nu_1\nu_2} \\ -\frac{\cos\phi}{\nu_1\nu_2} & \frac{1}{\nu_1^2} \end{bmatrix} \begin{bmatrix} y_1 \\ y_2 \end{bmatrix}$$

where $\phi = \phi_1 - \phi_2$. The eigenvector corresponding to the smaller eigenvalue is the major axis and its slope is the inverse of the intersection point as in Fig 3. Finally, note that the transfer function, (12) contains all the necessary information.

Consider two extreme cases where the ankle noise is zero (only hip noise; $w_1 = 0$ and $\sigma_r = 0$) and the hip noise is zero (only ankle noise; $w_2 = 0$ and $\sigma_r = \infty$). For example, when hip noise is zero, substituting $s = i\Omega$,

$$\frac{y_1}{w_1}(i\Omega) = H_{11}(i\Omega), \frac{y_2}{w_1}(i\Omega) = H_{21}(i\Omega)$$

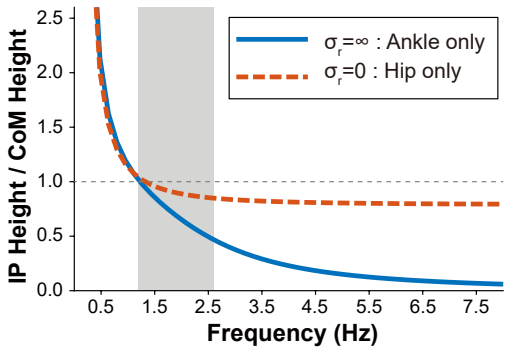

Figure 6 Height of the intersection point of the linearized double inverted pendulum model with two extreme σ_r values: $\sigma_r = 0$ (hip noise only) and $\sigma_r = \infty$ (ankle noise only).

and

$$\nu_1 = |H_{11}(i\Omega)|, \phi_1 = \angle H_{11}(i\Omega),$$
$$\nu_2 = |H_{21}(i\Omega)|, \phi_2 = \angle H_{21}(i\Omega).$$

The intersection point height can be calculated using the method above at different frequencies as shown in Fig. 6.

Since we are examining a linearized model, we can infer that the true response with both non-zero ankle and hip noise would be some combination of these two extreme responses.

List of abbreviations

LQR: linear quadratic regulator

CoP: center of pressure

IP: intersection point

CoM: center of mass

Declarations

Ethics approval and consent to participate

Not applicable.

Consent for publication

Not applicable.

Availability of data and materials

Not applicable.

Competing interests

The authors declare that they have no competing interests.

Funding

This work was supported in part by NSF-CRCNS 1724135, awarded to Neville Hogan and NSF-CRCNS-1723998, awarded to Dagmar Sternad. Jongwoo Lee was supported by a Samsung Scholarship.

Author's contributions

KS performed simulation and data analysis and drafted the manuscript. JL developed simulations and performed mathematical analysis of the intersection point. MR contributed to the frequency analysis of the intersection point. JL, MR, DS, and NH contributed to data and statistical analyses. KS and JL generated figures. All authors edited, read and approved the final manuscript.

Acknowledgements

Not applicable.

Author details

[1]Department of Mechanical Engineering, Massachusetts Institute of Technology, Cambridge, MA 02139, USA. [2]Department of Brain and Cognitive Science, Massachusetts Institute of Technology, Cambridge, MA 02139, USA. [3]Department of Biology, Northeastern University, Boston, MA 02115, USA. [4]Department of Electrical and Computer Engineering, Northeastern University, Boston, MA 02115, USA. [5]Department of Physics, Northeastern University, Boston, MA 02115, USA.

References

1. Peterka RJ. Sensorimotor Integration in Human Postural Control. Journal of Neurophysiology. 2002;88(3):1097–1118.
2. Allen JL, Ting LH. Why Is Neuromechanical Modeling of Balance and Locomotion So Hard? In: Prilutsky BI, Edwards DH, editors. Neuromechanical Modeling of Posture and Locomotion. New York: Springer; 2016. p. 197–223.
3. Horak FB. Postural orientation and equilibrium: What do we need to know about neural control of balance to prevent falls? In: Age and Ageing; 2006. p. ii7–ii11.
4. Collins JJ, De Luca CJ. Open-loop and closed-loop control of posture: A random-walk analysis of center-of-pressure trajectories. Experimental Brain Research. 1993;95:308–318.
5. Moon J, Pathak P, Kim S, Roh Sg, Roh C, Shim Y, et al. Shoes with active insoles mitigate declines in balance after fatigue. Scientific Reports. 2020;10:1–11.
6. Boehm WL, Nichols KM, Gruben KG. Frequency-dependent contributions of sagittal-plane foot force to upright human standing. Journal of Biomechanics. 2019;83:305–309.
7. Yamagata M, Gruben K, Falaki A, Ochs WL, Latash ML. Biomechanics of Vertical Posture and Control with Referent Joint Configurations. Journal of Motor Behavior. 2020;.
8. Gruben KG, Boehm WL. Force direction pattern stabilizes sagittal plane mechanics of human walking. Human Movement Science. 2012;31:649–659.
9. Maus HM, Lipfert SW, Gross M, Rummel J, Seyfarth A. Upright human gait did not provide a major mechanical challenge for our ancestors. Nature Communications. 2010;1.

10. Todorov E, Jordan MI. Optimal feedback control as a theory of motor coordination. Nature Neuroscience. 2002;5:1226–1235.
11. Todorov E. Optimality principles in sensorimotor control. Nature Publishing Group; 2004.
12. Kuo AD, Zajac FE. Human standing posture: Multi-joint movement strategies based on biomechanical constraints. Progress in Brain Research. 1993;97:349–358.
13. Kuo AD. An Optimal Control Model for Analyzing Human Postural Balance. IEEE Transactions on Biomedical Engineering. 1995;42:87–101.
14. Morasso P, Cherif A, Zenzeri J. Quiet standing: The Single Inverted Pendulum model is not so bad after all. PLOS ONE. 2019;14(3).
15. Loram ID, Lakie M. Direct measurement of human ankle stiffness during quiet standing: The intrinsic mechanical stiffness is insufficient for stability. John Wiley & Sons, Ltd; 2002.
16. Sontag ED. Mathematical Control Theory. vol. 6 of Texts in Applied Mathematics. New York, NY: Springer New York; 1998.
17. De Leva P. Adjustments to Zatsiorsky-Seluyanov's segment inertia parameters. Journal of biomechanics. 1996;29(9):1223–1230.
18. Duarte M, Sternad D. Complexity of human postural control in young and older adults during prolonged standing. Experimental Brain Research. 2008;191(3):265–276.
19. Horak FB, Nashner LM. Central programming of postural movements: Adaptation to altered support-surface configurations. Journal of Neurophysiology. 1986;55(6):1369–1381.
20. Nashner LM, McCollum G. The organization of human postural movements: A formal basis and experimental synthesis. Behavioral and Brain Sciences. 1985;8(1):135–150.
21. Runge CF, Shupert CL, Horak FB, Zajac FE. Ankle and hip postural strategies defined by joint torques. Gait and Posture. 1999;10(2):161–170.
22. Kiemel T, Zhang Y, Jeka JJ. Identification of neural feedback for upright stance in humans: Stabilization rather than sway minimization. Journal of Neuroscience. 2011;31(42):15144–15153.
23. Jones KE, Hamilton AFdC, Wolpert DM. Sources of signal-dependent noise during isometric force production. Journal of Neurophysiology. 2002;88(3):1533–1544.
24. Morasso PG, Schieppati M. Can muscle stiffness alone stabilize upright standing? Journal of Neurophysiology. 1999;82(3):1622–1626.
25. Winter DA, Patla AE, Rietdyk S, Ishac MG. Ankle muscle stiffness in the control of balance during quiet standing. Journal of Neurophysiology. 2001;85(6):2630–2633.
26. Kiemel T, Oie KS, Jeka JJ. Multisensory fusion and the stochastic structure of postural sway. Biological Cybernetics. 2002;87(4):262–277.
27. Rozendaal LA, Van Soest AJ. Stabilization of a multi-segment model of bipedal standing by local joint control overestimates the required ankle stiffness. Elsevier; 2008.
28. Yamamoto A, Sasagawa S, Oba N, Nakazawa K. Behavioral effect of knee joint motion on body's center of mass during human quiet standing. Gait and Posture. 2015;41(1):291–294.
29. Müller R, Rode C, Aminiaghdam S, Vielemeyer J, Blickhan R. Force direction patterns promote whole body stability even in hip-flexed walking, but not upper body stability in human upright walking. Proceedings of the Royal Society A: Mathematical, Physical and Engineering Sciences. 2017;473(2207).
30. Torres-Oviedo G, Ting LH. Muscle synergies characterizing human postural responses. Journal of Neurophysiology. 2007;98(4):2144–2156.